A needle-free transdermal patch for sampling interstitial fluid

Daniel J. O'Brien, Darrian Mills, Joseph Farina, Makarand Paranjape

Abstract—Objective: Modern diagnostics is pivoting towards less invasive health monitoring in dermal interstitial fluid, rather than blood or urine. However, the skin's outermost layer, the stratum corneum, makes accessing the fluid more difficult without invasive, needle-based technology. Simple, minimally invasive means for surpassing this hurdle are needed. Methods: To address this problem, a flexible, Band-Aid-like patch for sampling interstitial fluid was developed and tested. This patch uses simple resistive heating elements to thermally porate the stratum corneum, allowing the fluid to exude from the deeper skin tissue without applying external pressure. Fluid is then transported to an on-patch reservoir through selfdriving hydrophilic microfluidic channels. Results: Testing with living, ex-vivo human skin models demonstrated the device's ability to rapidly collect sufficient interstitial fluid for biomarker quantification. Further, finite-element modeling showed that the patch can porate the stratum corneum without raising the skin's temperature to paininducing levels in the nerve-laden dermis. Conclusion: Relying only on simple, commercially scalable fabrication methods, this patch outperforms the collection rate of various microneedle-based patches, painlessly sampling a human bodily fluid without entering the body. Significance: The technology holds potential as a clinical device for an array of biomedical applications, especially with the integration of on-patch testing.

Index Terms—flexible devices, microfluidics, interstitial fluid, opioid detection, transdermal diagnostics

I. INTRODUCTION

THE current medical practice for diagnosing, tracking, and treating many disease conditions requires biomarker monitoring in bodily fluids, typically blood or urine. The

Submitted 04 December 2022. The authors thank J. Nijdam and L. Der for their guidance in device fabrication. We thank I. Isayeva and members of the Center for Devices and Radiological Health at the U.S. FDA for insightful conversations regarding opioids and device regulation. We thank F. Rubinson, K. Knope, and S. Jilani for informative support of electrochemical experiments. We thank E. Van Keuren for use and support of COMSOL Multiphysics. We also thank the NSF for support through Award #1938995. We acknowledge the Georgetown Histopathology and Tissue Shared Resource for histology support and the Georgetown Mass Spectrometry and Analytical Pharmacology Shared Resource for LC-MS support and data collection. Lastly, we acknowledge Georgetown's cleanroom facility, GNuLab, in which the device was fabricated and characterized.

D. J. O'Brien was with the Department of Physics, Georgetown University, Washington, DC 20057 USA. He is now with Energy Innovation Policy and Technology LLC, San Francisco, CA 94111 USA (e-mail: djo44@georgetown.edu).

D. Mills, J. Farina, and M. Paranjape are with the Department of Physics, Georgetown University, Washington, DC 20057 USA (e-mail: paranjam@georgetown.edu).

effectiveness of these techniques is often limited by their collection: urine testing can be intrusive and has well-documented methods of sample tampering [1]; finger pricks are painful; and blood draws require medical visits and time-consuming post-processing. As an alternative, researchers have turned to health monitoring in interstitial fluid (ISF).

ISF is the extracellular fluid that lies between blood vessels and tissues in the body. It acts as a reservoir and transportation system that provides nutrients to tissues while also removing cellular metabolic waste. The endothelial cells that comprise capillaries are separated by intercellular clefts, 40–60-Å-wide channels that allow bidirectional passage of molecules smaller than 60 kDa [2], [3]. As a result of this process, called capillary exchange, ISF's composition largely mirrors that of blood plasma, but without larger constituents [4].

Microneedles are becoming the most popular technology for sampling ISF. Typically ranging from 0.2–2 mm in length, these devices can puncture into the dermis skin layer but are less invasive than typical hypodermic needles, including those used with continuous glucose monitors (CGMs) [5]. Microneedle-based devices can be designed to extract biofluids transdermally [6]. Multiple extraction mechanisms have been realized [7], including by capillary action through microneedles that are hollow [8] or porous [9], by adding suction [10], by ISF diffusion into hydrogel microneedles [11], and by osmotically-driven transport into osmolyte-filled microneedles [12]. On other testing platforms, microneedles themselves act as embedded electrodes [13] or conduct onneedle quantification of biomarkers [14].

Although microneedles are often referred to as a noninvasive solution, they nonetheless penetrate the skin and are not pain-free. The dermis contains nerve endings, and the pain associated with insertion of microneedle-based devices scales with the length and the number of needles in an array [15]. Furthermore, they are susceptible to fracture and, as the physics of lying on a bed of nails illustrates, arrays of microneedles can require significant insertion force [16].

Needle-free techniques for reaching dermal ISF often work by thermally porating the stratum corneum (SC), the outermost barrier layer of flattened, dehydrated skin cells. The SC can be permeated using pulsed lasers [17] to increase drug diffusion through the skin [18], [19] or collect ISF [20]. However, such lasers are typically bulky and impossible to integrate into lab-on-a-chip technologies for point-of-care applications. Superheated steam has also been proposed as a means to ablate tissue [21], but this technology is similarly complicated, requiring on-chip water reservoirs to function. Iontophoretic

devices, which use an electric field to extract constituents from the interstitial space [22], were at one point approved by the FDA but have since been pulled from the market because of issues including skin irritation, burns, and inadvertent shutdown during critical periods of hypoglycemia [23].

Our group has developed a wearable device for painlessly and noninvasively sampling ISF. The patch features an array of resistive heating elements ("microheaters") that each thermally ablate a small area of the SC, through which ISF can exude and be collected in the device. Similar heaters have been built into implantable [24] and transdermal devices [25]-[28] for drug delivery. Our device generates extreme temperature gradients by heating the skin surface at high temperatures (> 130 °C) for short times ($\ll 1$ s). Using preliminary modeling and in-vitro experimental verification, we previously showed the heaters' ability to generate pores in cultured human tissue [29], [30]. The first-generation patch used colorimetric detection to study ISF-glucose levels [25]. The second-generation patch pivoted to enzymatic electrochemical monitoring of glucose and lactate. In a pilot trial with this patch iteration (N = 10;M/F adults), participants reported no pain or sensations during micropore formation, but the device suffered from unreliability due to the rigid and brittle device materials (including glass, silicon, and SU-8 photoresist) [31].

With these issues in mind, we have re-designed the device, tailoring its fabrication process to be compatible with flexible materials. We test this new device with living, ex-vivo human skin models that better reproduce natural skin's morphology and heating response than is possible with either cultured human skin or animal studies. We make the first experimental measurement of the ISF volume collectable by thermal skin poration and compare it with that of popular microneedlebased techniques. Furthermore, we use 3D modeling to quantitatively characterize the ablation process and elucidate parameters that would result in replicable pain-free poration by ensuring that the temperature at the dermal nerve endings is sufficiently below the pain threshold. Lastly, having already used the device to monitor glucose and lactate with clinicallyrelevant accuracy, we now pivot to another application—opioid monitoring. Monitoring of opioid abuse is typically conducted with intrusive urine testing, and would benefit from a simpler sampling technique. Here, we utilize electrochemistry and mass spectrometric studies of the harvested ISF to demonstrate the potential for noninvasive biomolecular monitoring in an alternative human body fluid with our device.

II. EXPERIMENTAL METHODS

A. Materials

50- μ m-thick Kapton HN sheets were purchased from CS Hyde; Sylgard 184 polydimethylsiloxane (PDMS) was purchased from Fisher; meconin and 6-monoacetylmorphine (6-MAM) were purchased from Cayman; Whatman (Grade 1) filter papers, Trichloro(1H,1H,2H,2H-perfluorooctyl)silane (FOTS), (3-Mercaptopropyl)trimethoxysilane (MPTMS), and (3-Glycidyloxypropyl)trimethoxysilane (GPTMS) were purchased from Sigma-Aldrich; 23-mm NativeSkin models were purchased from Genoskin (3 donors, age = 35 \pm 8 years,

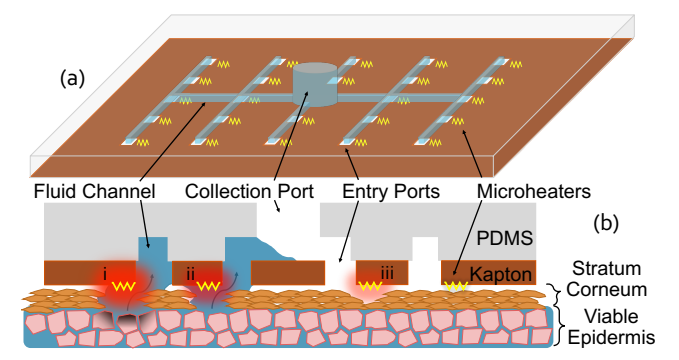


Fig. 1: Device schematic in (a) 3-D and (b) 2-D cross-sectional views

Fitzpatrick skin types 2–4, BMI = 30 ± 4); silicon and soda lime glass wafers were purchased from University Wafer; poly(dimethylsiloxane-b-ethylene oxide) (25:75) (PDMS-b-PEO) was purchased from Polysciences; TFA, TFN, and TFT etchants were purchased from Transene; HARE SQ-50 was purchased from KemLab; S1813 was purchased from Kayaku; and Au working, Pt wire counter, and Ag/AgCl reference electrodes were purchased from CH Instruments.

B. Device Design & Fabrication

The proposed device features two structural layers, each composed of a different flexible polymer: Kapton or PDMS. The Kapton side is placed in contact with the skin and has an array of 100 integrated gold microheaters along with ports through which sampled ISF can enter the device (Fig. 1). The voltage pulse applied across the microheaters is tuned experimentally; Fig. 1b illustrates how improperly tuning the pulse can (i) burn or (iii) underheat the skin; (ii) shows ISF flowing through a properly ablated pore. Once in the patch, ISF can then pass through microfluidic channels in the PDMS layer to a reservoir for collection and on- or off-patch testing.

To enable reliable processing, the flexible Kapton film was first attached to a rigid silicon handle wafer using a 20 μ m PDMS interlayer following the method of Sundani *et al.* [32]. The interlayer and Kapton were both treated with oxygen plasma then bonded together for 2 hours at 100 °C. This process allowed the Kapton to sit flush with a flat wafer then to be peeled after lithographic processing.

A 100-Å-thick chromium adhesion layer, followed by a 2500-Å gold thin film, was sputtered onto the Kapton and patterned into microheaters with standard Shipley 1813 photolithography. The metals were then etched with TFA and TFN etchants, respectively. A 7000-Å-thick titanium hard mask was then sputtered atop the heater side of the Kapton and patterned with Shipley 1813 and a dark-field mask. This mask delineated the capillary ports to be etched through the Kapton. The Ti was then etched with TFT etchant. Finally, the ports were dry etched through the Kapton layer in a Plasmalab80Plus at 240 mTorr and 300 W, with four successively alternating 30-minute O_2 and 30-second O_2/SF_6 steps.

The PDMS layer was fabricated using 2-layer negative photoresist molding. A 40-µm-thick SQ-50 layer was spun



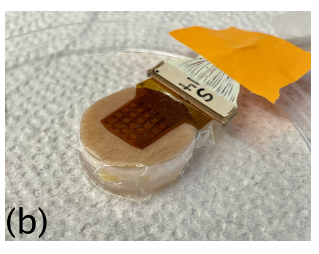


Fig. 2: (a) Six 23-mm-diameter NativeSkin models in a culture plate and (b) a single skin model with device attached via a Tegaderm film dressing, and connected to power supply with edge connector cabling

then patterned (but not developed), followed by a 100-µm-thick layer patterned with a separate mask. The thinner layer's mask defined the capillaries, while the thicker defined the ISF collection reservoir. After development, the mold was vaporphase silanized in a desiccator with 15 µL FOTS and 10 µL DI H₂O under rough vacuum. Sylgard 184 PDMS in a standard 10:1 ratio was mixed with 1 wt.% PDMS-b-PEO surfactant, then degassed, poured over the silanized mold, and cured at room temperature for 48 hours [33]. Subsequently, this hydrophilic PDMS was further cured at 65 °C for 2 hours. The Modulus of the PDMS formulation was determined with an Instron mechanical tester.

The PDMS and Kapton layers were peeled from their wafers and bonded using vapor-phase MPTMS and GPTMS as described by Hoang *et al.* [34]. Kapton was taped to a clean silicon wafer and PDMS adhered to a glass handle wafer, bond-sides-up. Each was then treated with oxygen plasma, and a monolayer of MPTMS (PDMS) or GPTMS (Kapton) was vapor deposited in a desiccator under rough vacuum. The layers were subsequently mounted in an aligner-stacking station and lubricated with 100 µL methanol to allow alignment before bonding on the heated stage at 50 °C overnight. Features on the Kapton layer were easily visible through the transparent PDMS/glass wafer for alignment.

More details on the development of the device's fabrication process are available in Ch. 4 of the author's PhD thesis [35].

C. Ex-vivo skin tests

The devices were tested using NativeSkin *ex-vivo* human skin models from Genoskin. These biopsies provide a safe alternative that closely mirrors testing on a living subject. The skin models, shown in Fig. 2, were cultured according to Genoskin's protocol. The patch device was attached to the skin using Tegaderm transparent film dressing (Fig. 2b). Heater resistances were measured, then devices were powered with a chosen voltage and pulse time, as controlled by a DC power supply and 555-timer circuit, respectively.

The widespread availability, low cost, and high absorbency of Whatman filter paper have enabled its use in ISF collection devices [36]; it was therefore used to determine the volume of fluid extracted from NativeSkin models, following protocol from Kim *et al.* [37]. Briefly, the area of a 4 x 14 mm filter paper wetted by 0.4–4 µL dyed PBS was calculated with Fiji and used to plot a calibration curve [38]. From this curve, the

volume of ISF collected from each NativeSkin model could be calculated by the area of a 2 x 7 filter paper that was wetted. This method was chosen both for simplicity and accuracy compared with, for example, measuring a mass change of the device before and after ISF collection, which is susceptible to evaporation issues.

After ablation studies, select tissues were fixed in 10% formalin for 24–48 hours, then embedded and sectioned. 5-µmthick sections at regular intervals across the tissue were stained with H&E for microscopy. Ablation profiles at varying pulse parameters were measured with H&E sections and compared with COMSOL simulations to connect ablation depth with skin temperatures.

D. Modeling

The thermal ablation process was modeled with COMSOL using a five-layer column geometry consisting of two device layers (Kapton, PDMS) and three skin layers (stratum corneum, viable epidermis, and dermis). A lone gold microheater was situated between the bottom of the device and the outermost skin layer. This setup is illustrated in Fig. S1, Supporting Information.

Using relevant material parameters (Table S1, Supporting Information) and boundary/initial conditions, Joule heating and heat transfer simulations rendered 3D thermal profiles corresponding to particular pulse durations and voltage drops across the microheater. These temperature profiles were used to determine the optimal conditions for skin ablation.

Lastly, whereas simulations were conducted with a potential applied directly across a single resistive unit, the patch device also contains interconnect traces with their own resistances. The protocol by which experiments were bridged with computational results is provided in the supporting document (Fig. S2, Supporting Information).

E. Voltammetric Tests

As a proof-of-principle application for ISF sampled with the device, the electrochemical properties of two heroin metabolites, meconin and 6-MAM, were tested using cyclic (CV) and square-wave voltammetry (SWV) in PBS at biological pH 7.4. These metabolites are specific markers of illicit heroin use and remain in biofluids like ISF much longer than heroin does, allowing for a longer testing window [39]. Detection with painlessly sampled ISF provides an advantage over intrusive urine testing for rehab and drug monitoring programs.

Voltammetry experiments were conducted under N_2 prebubbled through water to minimize evaporation. A gold working electrode, a platinum wire counter electrode, and a Ag/AgCl reference electrode were used. 1 mg mL⁻¹ meconin (5.15 mM) and 6-MAM (3.06 mM) solutions were prepared in PBS 1X. Stock was then added sequentially to pure PBS, while SWVs were taken from -0.1–1.0 V at 4 mV s⁻¹ and 25 mV pulse size. CVs were taken from -0.4–1.0 V with scan rate 100 mV s⁻¹.

F. Liquid Chromatography-Mass Spectrometry (LC-MS)

LC-MS was used for off-line analysis of ISF sampled from NativeSkin tissues. This sensing technique can provide more precise detection of molecules and can be used to detect non-electrochemically active opioid metabolites.

The culture media of specific NativeSkin models was spiked with 0.5 mg mL $^{-1}$ meconin and 0.5 mg mL $^{-1}$ 6-MAM. The models were left in culture for 2 hours, then ISF was extracted from the tissues by SC thermal ablation with the device. The ISF was then collected from the device using filter papers, which were subsequently placed in 200 μL DI H_2O and stored at -80 °C until testing. Targeted LC-MS metabolomics was used to quantify the concentration of 6-MAM and meconin found in the ISF. Multiple reaction monitoring analyses were performed using transitions at m/z 327.8 \rightarrow 165.1 for 6-MAM and 195 \rightarrow 180 for meconin. Detailed LC-MS experimental procedures are available in the supporting document.

III. RESULTS & DISCUSSION

A. Device Processing

A fully fabricated device is shown in Fig. 3a. The gold microheaters, located on the device's Kapton face have a trace width of 6 μ m and a meandering length of 650 μ m (Fig. S3, Supporting Information). The ISF access ports etched through the Kapton are 100 μ m-square, and allow the fluid to enter the PDMS microfluidic channel network (Fig. 3b). For etching, an alternating O₂ and O₂/SF₆ plasma sequence was chosen to balance etch rate with selectivity—although SF₆ etches Kapton more quickly, it also rapidly erodes the lithographically patterned Ti hard mask [40].

The PDMS layer features a series of 50-µm-wide, 40-µm-tall channels, leading from the 25 heating sites to a central reservoir, from which interstitial fluid can be collected for analysis (Fig. 3c-d). The microfluidic layer was made by casting uncured PDMS over a lithographically patterned photoresist mold, then curing it. Vapor-deposited FOTS was used to silanize the mold for easier PDMS delamination. After silanization, water contact angles on the mold's silicon wafer and photoresist increased from 23° to 109° and 71° to 142°, respectively (Fig. S4, Supporting Information), matching values from the literature [41], [42]. This hydrophobicity arises from the low packing density of fluorocarbons on the surface, resulting in poor Van der Waals interactions [43].

Before curing, PDMS was mixed with PDMS-b-PEO surfactant to make the resulting fluidic channels hydrophilic [44]. When ISF is introduced to the PDMS channels, surfactant migrates to the channel walls to induce autonomous wetting, allowing capillary fluid flow without external pumping [33], [45], [46]. Originally, the PDMS was cured at 65 °C for 4 hours, but the polymer undergoes cure temperature-dependent shrinkage, which can cause misalignment of features during bonding [47]. Instead, the PDMS was cured at room temperature to its gelation point, then the curing was completed safely at 65 °C without shrinkage.

Finally, the Kapton and PDMS layers were bonded together using a custom-built stacking station. A methanol lubrication layer between the two polymers allowed features in the layers

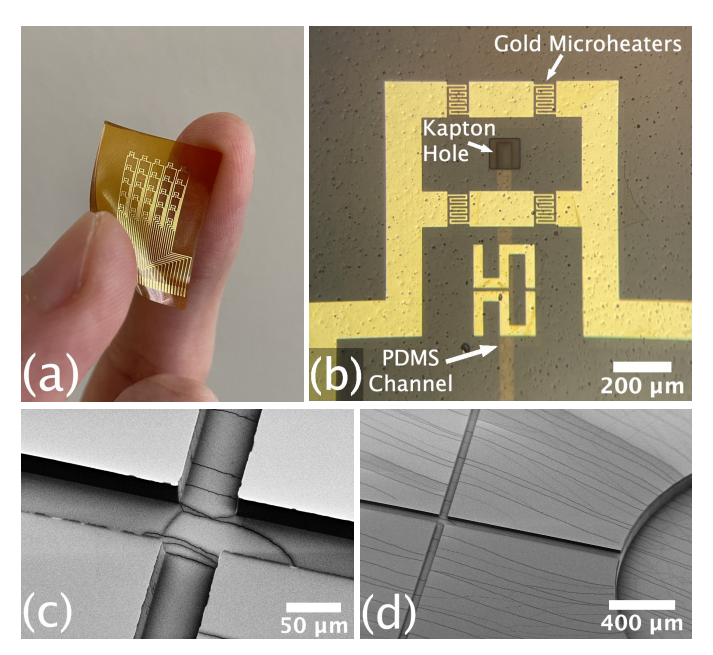
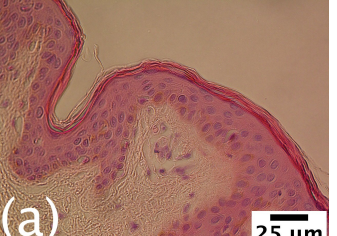
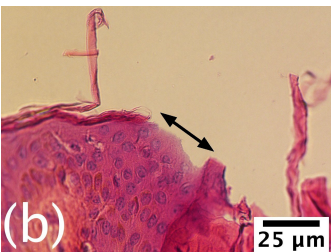


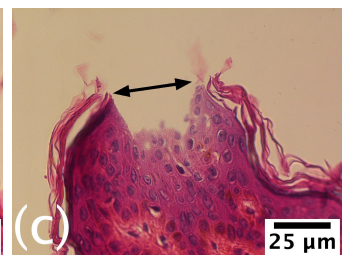
Fig. 3: (a) Photo of a fully fabricated device; (b) a micrograph showing a device heating site, including gold microheaters and a PDMS channel aligned with an ISF entry port, visible through the Kapton layer; SEM of (c) PDMS microchannels and (d) ISF collection channels/reservoir (visible cracking is actually the gold film used for imaging)

to be aligned without inadvertent bonding. Once aligned, the two were irreversibly bonded through a click reaction between monolayers of MPTMS and GPTMS on the heated stage of the stacking station at 50 °C. On attempting to separate the bonded layers, PDMS underwent cohesive failure in the bulk rather than adhesive failure at the interface, indicating permanent, strong bonding (Fig. S5, Supporting Information).

The device and materials were bench tested to evaluate reproducibility throughout development. The Modulus of the 1% surfactant PDMS (2.9 \pm 0.2 MPa) matched expected values from the literature [48]. The dynamic hydrophilic nature of the surfactant-PDMS was confirmed with contact angle goniometry, as reported by our group previously [33], and liquids introduced to the surface of the patch could be observed flowing through the microchannels autonomously, further validating the hydrophilizing mechanism. The Cr/Au heaters were evaluated with resistance measurements, which confirmed both the continuity of the wires and the uniformity of heaters across a device. Early in device development, these measurements elucidated a flaw in our fabrication process the radial dependence of the deposition rate in our sputterer caused varying heater resistances across a wafer (Fig. S6, Supporting Information). This problem is readily solved with more advanced deposition technology, but should be noted in small-facility batch processing. Simulated aging tests, conducted by repeatedly bending the flexible Kapton substrate (Fig. S7, Supporting Information), resulted in no appreciable change in heater resistance. Tests with more advanced probing equipment that better measures changes in low-resistance systems will be conducted in future studies.







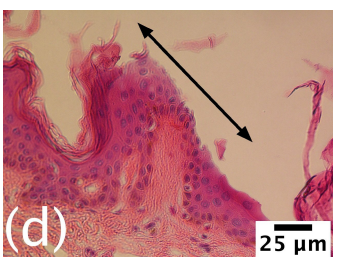


Fig. 4: H&E-stained NativeSkin sections showing (a) healthy skin and skin ablated at 4 V applied potential for (b) 34 ms, (c) 150 ms, and (d) 1000 ms

B. Ex-vivo skin tests

The devices were tested with ex-vivo human skin models to determine 1) the skin ablation depth at varying microheater electrical parameters; and 2) the fluid volume exuded through the resulting pores. The potential applied to the device was controlled with a DC power supply and 555-timer circuit to allow for pulse widths between 16-480 ms or manually for longer pulse durations (e.g., 1 s). The ablation depth from microheater pulses scaled with the applied potential and pulse time. Fig. 4 shows this relationship for 34-, 150-, and 1000-ms pulses at a device potential of 4.0 V. At short times, ablation was primarily limited to the SC. Alternatively, penetration into the stratum spinosum layer of the viable epidermis (VE) was present after 150-ms-long pulses. After a 1000-ms pulse, large areas of the skin were ablated down to the stratum basale, indicating the presence of explosive water vaporization events within the epidermis.

As demonstrated, it is critical to tune the thermal energy delivered to the skin in order to avoid lasting tissue damage. These experiments are not possible within human trials, and care must be taken when translating animal trial results to medicine. Mice, for example, have thinner skin and fewer epidermal layers, and their wounds heal by different mechanisms than humans' (contraction vs. granulation) [49]. Pig skin is structurally similar to human skin, but with some histological and immunological differences [50]. *Ex-vivo* studies with models like NativeSkin therefore present critical steps forward in more accurate, cost-effective and ethical pilot studies for medical devices, especially in wound healing [51].

NativeSkin studies were also useful in determining the ISF volume exuded after microporation. First, the volume of PBS absorbed by Whatman filter paper *in vitro* was shown to be directly related to the area of the paper wetted (Fig. S8, Supporting Information). This calibration curve was used to calculate the volume of ISF collected from NativeSkin models after poration. An average of $0.014 \pm 0.002~\mu L$ of ISF per pore was collected across these samples (N = 6; > 1 $\mu L/patch$). Fig. 5 compares this value with that of various vacuum-free, microneedle-based techniques from Samant and Prausnitz [52]. Only 30-gauge microneedles collected a statistically greater volume of ISF per pore than our device (at a P < 0.05 level). However, data from the literature represented the volume collected over a 20-minute period, in contrast to our collection period of only 1 minute after ablation.

This rapid collection is likely due to the lack of transport

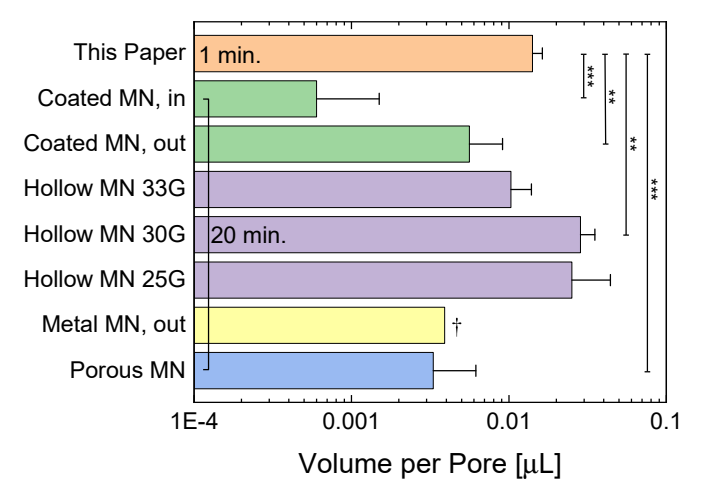


Fig. 5: Comparison of ISF volume collected by ablation vs. other methods from the literature [52]; data show mean \pm SD (n \geq 4); **P < 0.01, ***P < 0.001; †: SD not given

barriers found in ablated micropores. While much larger volumes of ISF would likely be collected by our device over 20 minutes (e.g., [52] saw a ~9-fold increase in collected volume after 20 minutes vs. after 1 minute), short use times better represent the real-world application of point-of-care devices.

These tests confirm the ability of the device to porate the stratum corneum, allowing access to the viable tissue below. In order to avoid infection, testing with living subjects should be preceded by ethanol sterilization. Methods for simultaneous delivery of antimicrobials during ablation-enabled fluid sampling have also been proposed [53], and microneedles are regularly used for local delivery of antimicrobials [54].

C. Modeling

Finite-element modeling using COMSOL demonstrated how short thermal pulses at properly tuned potentials can offer sufficient heat to ablate localized areas of the SC without raising temperatures in the nerve-laden dermis layer to pain-inducing levels (> 45 °C). For example, the temperature-depth curves in Fig. 6a show that below potentials of 0.6 V, a 34 ms pulse should be pain free. Fig. 6b, showing the time evolution of a 34-ms pulse temperature profile for a single potential, demonstrates the rapid drop in skin temperature after the potential is turned off. Fig. 6c, a 2D thermal profile, sliced vertically through the skin and device, shows how elevated

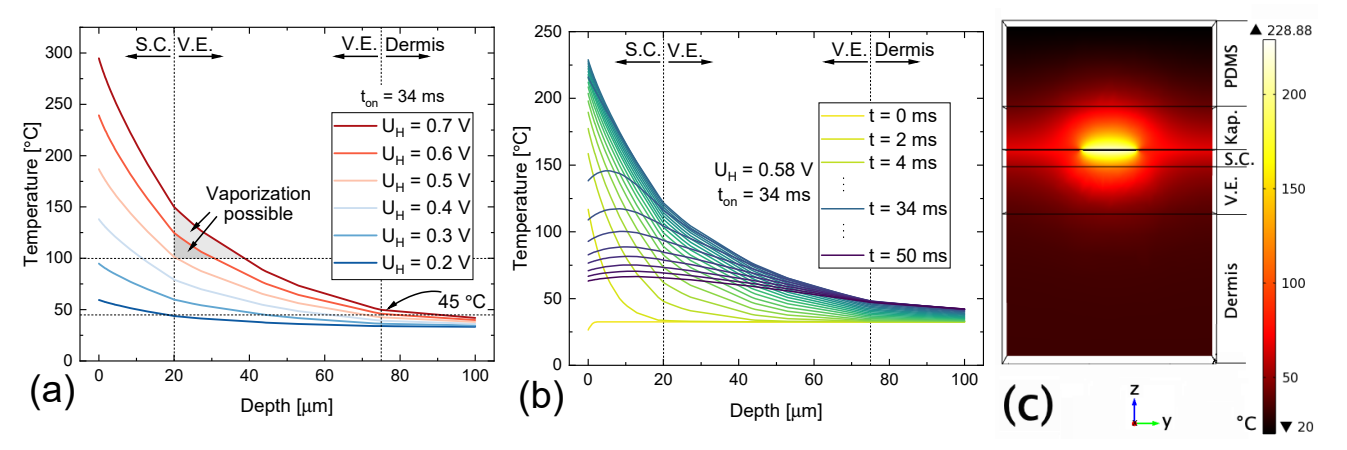


Fig. 6: (a) Temperature-depth profiles for 34-ms pulses at multiple heater potentials; (b) a time-evolution temperature-depth profile for a 34-ms pulse at 0.58 V heater potential; and (c) the corresponding y-z temperature slice at 34 ms

temperatures are restricted to the skin area immediately adjacent to the heater.

During experiments at higher potentials, microheating elements would often open circuit (Fig. S9a, Supporting Information). It was hypothesized that these failures arose due to stresses from thermal expansion of the Kapton and gold films. Thermal stress simulations in COMSOL (Fig. S9b–d, Supporting Information) showed that during 1000-ms pulses above potentials of approximately 0.6 V across the heater, the gold film underwent stress above its yield stress [55]. In order to avoid these stresses, it is important to limit heater temperatures to under ~350 °C (which also approaches the thermal stability limit of Kapton); notably, this is well above our anticipated operating temperature.

Four major thermal transitions have been identified in human stratum corneum between 0–100 °C: three associated with lipid fluidization and one with protein denaturation [56], [57]. Additionally, water vaporization takes place when the viable epidermis is heated to temperatures above 100 °C. Our simulations neglected the enthalpies associated with these phase changes.

After the ablation processes described above, up to ~ 30 mJ of energy per heater is dissipated within the skin, depending on pulse duration. Using previously reported enthalpy values [56], the energy absorbed by SC phase changes in the area adjacent to a heater was found to be $\sim 5~\mu J$. This value is much smaller than 30 mJ, thus it is safe to ignore these transitions. Alternatively, 0.5 mJ would be needed to vaporize water in the top 20 μ m of the VE. Therefore, the model could be improved by considering epidermal water vaporization for situations where the VE is heated significantly. As designed, the model may over-approximate heating in the deeper VE and dermis layers of the skin. Pulses at higher potentials may actually be safer than the model suggests from a pain perspective.

The model also ignores convective cooling in the skin by blood. At short times, heat transport in skin is typically characterized only by conduction [58]. Below an "effective time" of 15 seconds, Walters *et al.* showed that surface temperature after heating is nearly independent of blood perfusion [59]. Thus, neglecting convective cooling is a valid assumption.

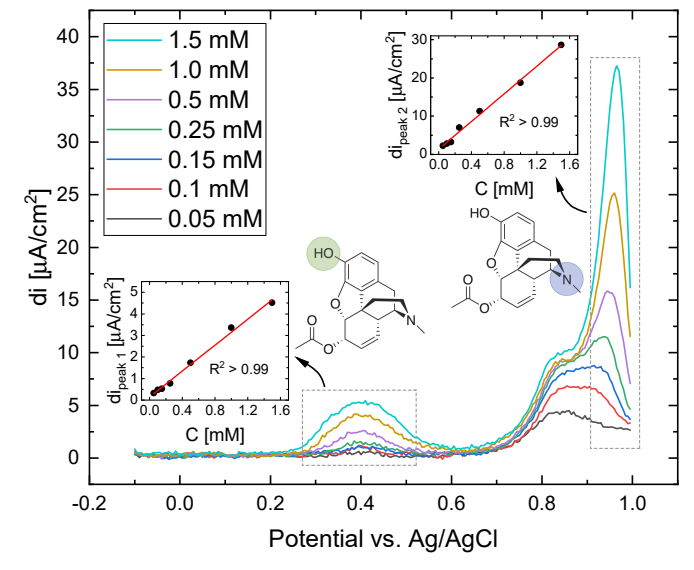


Fig. 7: SWVs of 6-MAM at pH 7.4. Inset plots show the current vs. concentration of each peak

D. Voltammetric Tests

Compared with CV, SWV was better able to identify electrochemical behavior under biological conditions because capacitive current is minimized by this technique (Fig. 7). CVs are shown in Fig. S10a, Supporting Information. Whereas meconin did not display activity within the aqueous solvent window, 6-MAM displayed oxidation peaks around +405 and +954 mV vs. Ag/AgCl. The voltage at peak current for both points was highly replicable, within \pm 3 and \pm 6 mV across the seven tested concentrations, respectively. The current at each of the two oxidative peaks increased linearly with concentration as shown in the figure insets. These calibration curves could be used for quantitative identification of 6-MAM in biological fluids such as ISF.

The peak at 405 mV corresponds to oxidation of the 6-MAM phenol group, while the peak at 954 mV corresponds to oxidation of the tertiary amine (mechanism akin to Rodriguez *et al.* [60]). The locations of the two peaks match expected

values from the literature [61]. The shoulder peak around ~850 mV is ascribed to further oxidation of the phenolic groups in dimerized 6-MAM (Fig. S10b, Supporting Information). Similar behavior has been observed in morphine voltammetry—generated pseudomorphine is further oxidized at approximately 800 mV [62].

In vivo, 6-MAM reaches a maximum plasma concentration of between 1731–5742 ng mL⁻¹ (5.3–17.6 μM) at 0.3–2.7 min after intravenous heroin administration [63]. With a half-life of 3–52 minutes, this molecule can feasibly be used for detecting illicit heroin use. However, comparing our data with the low concentrations found in plasma after administration, detection with mass spectrometry is likely to prove more effective.

E. Liquid chromatography-mass spectrometry

The levels of 6-MAM and meconin in ISF (from tissues spiked with the metabolites) were studied with targeted LC-MS analysis. The limit of detection (LOD) was 0.01 ng mL⁻¹ for 6-MAM and 0.1 ng mL⁻¹ for meconin. The lower limit of quantification (LLOQ) was 0.04 ng mL⁻¹ for 6-MAM and 0.1 ng mL⁻¹ for meconin. No metabolite saturation or sample-to-sample carryovers were observed in the quantification range. ISF showed mean concentrations of the metabolites at 0.046 and 0.042 mg mL⁻¹, respectively. These levels fall well within the detection range of the molecules. Thus, LC-MS analysis of ISF sampled from the patch presents a feasible path forward for monitoring opioid use less invasively than would be possible with blood or urine sampling.

IV. CONCLUSION

The difficulty of extracting ISF has traditionally limited the potential it holds for revolutionizing health monitoring. This study presents a flexible device that porates the skin to rapidly sample the fluid in sufficiently large, microliter-sized quantities for such tests. As shown through a combination of modeling and histological experiments, the device can systematically limit ablation to the stratum corneum skin layer, not damaging the viable layers below or causing pain-inducing temperatures in the nerve-laden dermis. Further, electrochemistry and mass spectrometry demonstrated the feasibility of biomarker monitoring in collected ISF. This paper reports one of the first technologies able to collect a measurable volume of dermal ISF without penetrating or applying vacuum to the skin. Moving forward, we aim to incorporate detection electrodes onto the device for in-situ electrochemical biomarker monitoring. Additionally, we plan to make the device microheaters wireless by employing inductive coupling with devices such as smartphones. Future NativeSkin studies should optimize ablation parameters for varying bodily locations, subject age, and skin color, and could examine pore closure time using transepidermal water loss technology, which could be important for determining infection risk.

REFERENCES

[1] W. B. Jaffee et al., "Is this urine really negative? a systematic review of tampering methods in urine drug screening and testing," *Journal of Substance Abuse Treatment*, vol. 33, no. 1, pp. 33–42, 2007.

- [2] C. G. Wermuth, The Practice of Medicinal Chemistry. Elsevier, 2003.
- [3] L. R. Johnson, Essential medical physiology. Elsevier, 2003.
- [4] J. Scallan, V. H. Huxley, and R. J. Korthuis, "Capillary fluid exchange: regulation, functions, and pathology," in *Colloquium Lectures on Integrated Systems Physiology: From Molecules to Function*, vol. 2. Morgan & Claypool Publishers, 2010, pp. 1–94.
- [5] N. Kashaninejad *et al.*, "Microneedle arrays for sampling and sensing skin interstitial fluid," *Chemosensors*, vol. 9, no. 4, p. 83, 2021.
- [6] E. Mukerjee et al., "Microneedle array for transdermal biological fluid extraction and in situ analysis," Sens. Actuators, A, vol. 114, no. 2-3, pp. 267–275, 2004.
- [7] A. Than, P. Zan, and P. Chen, "Transdermal theranostics," View, vol. 1, no. 2, p. e21, 2020.
- [8] P. R. Miller et al., "Extraction and biomolecular analysis of dermal interstitial fluid collected with hollow microneedles," Commun. Biol., vol. 1, no. 1, pp. 1–11, 2018.
- [9] K. Takeuchi et al., "Microfluidic chip to interface porous microneedles for isf collection," Biomed. Microdevices, vol. 21, no. 1, pp. 1–10, 2019.
- [10] P. M. Wang, M. Cornwell, and M. R. Prausnitz, "Minimally invasive extraction of dermal interstitial fluid for glucose monitoring using microneedles," *Diabetes Technol. Ther.*, vol. 7, no. 1, pp. 131–141, 2005.
- [11] J. Zhu et al., "Gelatin methacryloyl microneedle patches for minimally invasive extraction of skin interstitial fluid," Small, vol. 16, no. 16, p. 1905910, 2020.
- [12] M. Zheng et al., "Osmosis-powered hydrogel microneedles for microliters of skin interstitial fluid extraction within minutes," Adv. Healthcare Mater., vol. 9, no. 10, p. 1901683, 2020.
- [13] F. Tehrani et al., "An integrated wearable microneedle array for the continuous monitoring of multiple biomarkers in interstitial fluid," Nature Biomedical Engineering, pp. 1–11, 2022.
- [14] Z. Wang et al., "Microneedle patch for the ultrasensitive quantification of protein biomarkers in interstitial fluid," *Nature biomedical engineering*, vol. 5, no. 1, pp. 64–76, 2021.
- [15] H. S. Gill et al., "Effect of microneedle design on pain in human subjects," Clin. J. Pain, vol. 24, no. 7, p. 585, 2008.
- [16] S. P. Davis *et al.*, "Insertion of microneedles into skin: measurement and prediction of insertion force and needle fracture force," *J. Biomech.*, vol. 37, no. 8, pp. 1155–1163, 2004.
- [17] S. L. Jacques et al., "Controlled removal of human stratum corneum by pulsed laser," J. Invest. Dermatol., vol. 88, no. 1, pp. 88–93, 1987.
- [18] L. R. Sklar et al., "Laser assisted drug delivery: a review of an evolving technology," Lasers Surg. Med., vol. 46, no. 4, pp. 249–262, 2014.
- [19] C.-H. Lin, I. A. Aljuffali, and J.-Y. Fang, "Lasers as an approach for promoting drug delivery via skin," *Expert Opin. Drug Delivery*, vol. 11, no. 4, pp. 599–614, 2014.
- [20] M. Venugopal et al., "Clinical evaluation of a novel interstitial fluid sensor system for remote continuous alcohol monitoring," *IEEE Sens.* J., vol. 8, no. 1, pp. 71–80, 2008.
- [21] J. W. Lee et al., "Microsecond thermal ablation of skin for transdermal drug delivery," J. Controlled Release, vol. 154, no. 1, pp. 58–68, 2011.
- [22] M. J. Tierney et al., "The glucowatch® biographer: a frequent, automatic and noninvasive glucose monitor," Ann. Med., vol. 32, no. 9, pp. 632– 641, 2000.
- [23] S. K. Vashist, "Non-invasive glucose monitoring technology in diabetes management: A review," Anal. Chim. Acta, vol. 750, pp. 16–27, 2012.
- [24] J. Farina, M. Paranjape, and D. O'brien, "Implantable drug delivery using polycaprolactone with thermally triggerable release," *Bull. Am. Phys. Soc.*, vol. 66, 2021.
- [25] M. Paranjape et al., "A pdms dermal patch for non-intrusive transdermal glucose sensing," Sens. Actuators, A, vol. 104, no. 3, pp. 195–204, 2003.
- [26] A. V. Badkar et al., "Transdermal delivery of interferon alpha-2b using microporation and iontophoresis in hairless rats," *Pharm. Res.*, vol. 24, no. 7, pp. 1389–1395, 2007.
- [27] J. Bramson et al., "Enabling topical immunization via microporation: a novel method for pain-free and needle-free delivery of adenovirus-based vaccines," *Gene Ther.*, vol. 10, no. 3, pp. 251–260, 2003.
- [28] A. C. Sintov et al., "Radiofrequency-driven skin microchanneling as a new way for electrically assisted transdermal delivery of hydrophilic drugs," J. Controlled Release, vol. 89, no. 2, pp. 311–320, 2003.
- [29] E. Van Keuren et al., "Three dimensional thermal effects in mems devices," MRS Online Proc. Libr., vol. 687, no. 1, pp. 1–6, 2001.
- [30] ——, "Temperature profiles of microheaters using fluorescence microthermal imaging," Sens. Mater., vol. 17, no. 1, pp. 1–6, 2005.
- [31] S. Clement, C. DeWitt, and M. Paranjape, "Comparison of a new transdermal sensing device to the standard laboratory method for measuring glucose in type 1 diabetic patients," 7/12/2010–11/5/2010, IRB #2010-13. RX #4324-656.

- [32] H. Sundani et al., "Design and fabrication of a micromachined free-floating membrane on a flexible substrate," J. Micro/Nanolithogr., MEMS, MOEMS, vol. 12, no. 1, p. 013002, 2013.
- [33] D. J. O'Brien and M. Paranjape, "Modeling dynamic surface tension on surfactant-enhanced polydimethylsiloxane," *Langmuir*, vol. 37, no. 46, pp. 13610–13616, 2021.
- [34] M. V. Hoang, H.-J. Chung, and A. L. Elias, "Irreversible bonding of polyimide and polydimethylsiloxane (pdms) based on a thiol-epoxy click reaction," *J. Micromech. Microeng.*, vol. 26, no. 10, p. 105019, 2016.
- [35] D. J. O'Brien, "A painless, non-invasive, and flexible device to sample interstitial fluid for biomarker monitoring," Ph.D. dissertation, Georgetown University, Washington, DC, 2022.
- [36] C. Kolluru et al., "Recruitment and collection of dermal interstitial fluid using a microneedle patch," Adv. Healthcare Mater., vol. 8, no. 3, p. 1801262, 2019.
- [37] S. Kim *et al.*, "Enhanced extraction of skin interstitial fluid using a 3d printed device enabling tilted microneedle penetration," *Sci. Rep.*, vol. 11, no. 1, pp. 1–11, 2021.
- [38] J. Schindelin *et al.*, "Fiji: an open-source platform for biological-image analysis," *Nature Methods*, vol. 9, no. 7, pp. 676–682, 2012.
- [39] A. Maas, B. Madea, and C. Hess, "Confirmation of recent heroin abuse: Accepting the challenge," *Drug testing and analysis*, vol. 10, no. 1, pp. 54–71, 2018.
- [40] U. Buder, J.-P. Von Klitzing, and E. Obermeier, "Reactive ion etching for bulk structuring of polyimide," *Sens. Actuators*, A, vol. 132, no. 1, pp. 393–399, 2006.
- [41] P. Bryk et al., "What is the value of water contact angle on silicon?" Mater., vol. 13, no. 7, p. 1554, 2020.
- [42] T. M. Mayer et al., "Chemical vapor deposition of fluoroalkylsilane monolayer films for adhesion control in microelectromechanical systems," J. Vac. Sci. Technol., B: Microelectron. Nanometer Struct.— Process., Meas., Phenom., vol. 18, no. 5, pp. 2433–2440, 2000.
- [43] V. H. Dalvi and P. J. Rossky, "Molecular origins of fluorocarbon hydrophobicity," *Proc. Natl. Acad. Sci.*, vol. 107, no. 31, pp. 13603– 13607, 2010.
- [44] M. Yao and J. Fang, "Hydrophilic peo-pdms for microfluidic applications," J. Micromech. Microeng., vol. 22, no. 2, p. 025012, 2012.
- [45] D. J. O'Brien, A. J. Sedlack, and M. Paranjape, "Facile methods to make pdms hydrophilic: a time evolution study for microfluidic devices," in *IEEE Int. Conf. Micro Electro Mech. Syst. (MEMS)*. IEEE, 2020, pp. 346–349.
- [46] D. J. O'Brien et al., "Systematic characterization of hydrophilized polydimethylsiloxane," J. Microelectromech. Syst., vol. 29, no. 5, pp. 1216–1224, 2020.
- [47] S. W. Lee and S. S. Lee, "Shrinkage ratio of pdms and its alignment method for the wafer level process," *Microsystem technologies*, vol. 14, no. 2, pp. 205–208, 2008.
- [48] M. P. Wolf, G. B. Salieb-Beugelaar, and P. Hunziker, "Pdms with designer functionalities—properties, modifications strategies, and applications," *Progress in Polymer Science*, vol. 83, pp. 97–134, 2018.
- [49] H. D. Zomer and A. G. Trentin, "Skin wound healing in humans and mice: Challenges in translational research," *J. Dermatol. Sci.*, vol. 90, no. 1, pp. 3–12, 2018.
- [50] S. Debeer et al., "Comparative histology and immunohistochemistry of porcine versus human skin," Eur. J. Dermatol., vol. 23, no. 4, pp. 456– 466, 2013.
- [51] A. Liu et al., "Modeling early thermal injury using an ex vivo human skin model of contact burns," Burns, vol. 47, no. 3, pp. 611–620, 2021.
- [52] P. P. Samant and M. R. Prausnitz, "Mechanisms of sampling interstitial fluid from skin using a microneedle patch," *Proc. Natl. Acad. Sci.*, vol. 115, no. 18, pp. 4583–4588, 2018.
- [53] M. Paranjape and S. M. Paranjape, "Apparatus and method for delivery of antimicrobial during a transdermal sampling and delivery process," Jan. 11 2022, uS Patent 11,219,390.
- [54] R. Jamaledin et al., "Advances in antimicrobial microneedle patches for combating infections," Advanced Materials, vol. 32, no. 33, p. 2002129, 2020.
- [55] H. Espinosa and B. Prorok, "Size effects on the mechanical behavior of gold thin films," J. Mater. Sci., vol. 38, no. 20, pp. 4125–4128, 2003.
- [56] P. A. Cornwell *et al.*, "Modes of action of terpene penetration enhancers in human skin; differential scanning calorimetry, small-angle x-ray diffraction and enhancer uptake studies," *Int. J. Pharm.*, vol. 127, no. 1, pp. 9–26, 1996.
- [57] Y. Shahzad et al., "Breaching the skin barrier through temperature modulations," J. Controlled Release, vol. 202, pp. 1–13, 2015.
- [58] K. R. Foster et al., "Heating of tissues by microwaves: A model analysis," *Bioelectromagnetics*, vol. 19, no. 7, pp. 420–428, 1998.

- [59] T. J. Walters et al., "Heating and pain sensation produced in human skin by millimeter waves: comparison to a simple thermal model." Health Phys., vol. 78, no. 3, pp. 259–267, 2000.
- Phys., vol. 78, no. 3, pp. 259–267, 2000.
 [60] J. R. B. Rodríguez et al., "Voltammetric assay of heroin in illicit dosage forms," Analyst, vol. 115, no. 2, pp. 209–212, 1990.
- [61] J. Garrido et al., "Voltammetric oxidation of drugs of abuse iii. heroin and metabolites," *Electroanal.*, vol. 16, no. 18, pp. 1497–1502, 2004.
- [62] P. H. Jordan and J. P. Hart, "Voltammetric behaviour of morphine at a glassy carbon electrode and its determination in human serum by liquid chromatography with electrochemical detection under basic conditions," *Analyst*, vol. 116, no. 10, pp. 991–996, 1991.
- [63] E. J. Rook et al., "Pharmacokinetics and pharmacokinetic variability of heroin and its metabolites: review of the literature," Curr. Clin. Pharmacol., vol. 1, no. 1, pp. 109–118, 2006.